JOURNAL OF VIROLOGY, Feb. 2010, p. 1891–1901 Vol. 84, No. 4
0022-538X/10/$12.00 doi:10.1128/JVI.02458-09

A Single Tyrosine in the Severe Acute Respiratory Syndrome Coronavirus Membrane Protein Cytoplasmic Tail Is Important for Efficient Interaction with Spike Protein[▽]

Corrin E. McBride and Carolyn E. Machamer*

Department of Cell Biology, The Johns Hopkins University School of Medicine, Baltimore, Maryland 21205

Received 20 November 2009/Accepted 25 November 2009

Severe acute respiratory syndrome coronavirus (SARS-CoV) encodes 3 major envelope proteins: spike (S), membrane (M), and envelope (E). Previous work identified a dibasic endoplasmic reticulum retrieval signal in the cytoplasmic tail of SARS-CoV S that promotes efficient interaction with SARS-CoV M. The dibasic signal was shown to be important for concentrating S near the virus assembly site rather than for direct interaction with M. Here, we investigated the sequence requirements of the SARS-CoV M protein that are necessary for interaction with SARS-CoV S. The SARS-CoV M tail was shown to be necessary for S localization in the Golgi region when the proteins were exogenously coexpressed in cells. This was specific, since SARS-CoV M did not retain an unrelated glycoprotein in the Golgi. Importantly, we found that an essential tyrosine residue in the SARS-CoV M cytoplasmic tail, Y_{195}, was important for S-M interaction. When Y_{195} was mutated to alanine, M_{Y195A} no longer retained S intracellularly at the Golgi. Unlike wild-type M, M_{Y195A} did not reduce the amount of SARS-CoV S carbohydrate processing or surface levels when the two proteins were coexpressed. Mutating Y_{195} also disrupted SARS-CoV S-M interaction *in vitro*. These results suggest that Y_{195} is necessary for efficient SARS-CoV S-M interaction and, thus, has a significant involvement in assembly of infectious virus.

Coronaviruses are enveloped positive-strand RNA viruses that infect a wide variety of mammalian and avian species. These viruses generally cause mild disease in humans and are one major cause of the common cold (34). However, severe acute respiratory syndrome coronavirus (SARS-CoV), a novel human coronavirus which emerged in the Guangdong province in China in 2002 (30, 48), caused a widespread pandemic. SARS-CoV caused severe disease with a mortality rate of approximately 10%, the highest for any human coronavirus to date (62). The phylogeny and group classification of SARS-CoV remain controversial (17), but it is widely accepted to be a distant member of group 2. While SARS-CoV is no longer a major health threat, understanding the basic biology of this human pathogen remains important.

Coronaviruses encode three major envelope proteins in addition to various nonstructural and accessory proteins. The envelope protein (E) is the least abundant structural protein in the virion envelope, although it is expressed at robust levels during infection (21). E plays an essential role in assembly for some but not all coronaviruses (31–33, 45) and may also be a viroporin (reviewed in reference 21). The spike glycoprotein (S) is the second most abundant protein in the envelope. S determines host cell tropism, binds the host receptor, and is responsible for virus-cell, as well as cell-cell, fusion (15). The S protein is a type I membrane protein with a large, heavily glycosylated luminal domain and a short cytoplasmic tail that has been shown to be palmitoylated in some coronaviruses (47, 58). The membrane protein (M) is the most abundant protein in the virion envelope and acts as a scaffold for virus assembly. M has three transmembrane domains, a long cytoplasmic tail, and a short glycosylated luminal domain (reviewed in reference 21). Unlike many enveloped viruses, coronaviruses assemble at and bud into the lumen of the endoplasmic reticulum (ER)-Golgi intermediate compartment (ERGIC) and exit the infected cell by exocytosis (29). In order to accomplish this, the envelope proteins must be targeted to the budding compartment for assembly.

For most coronaviruses, the E and M proteins localize in the Golgi region near the budding site independently of other viral structural proteins. We have previously shown for infectious bronchitis virus (IBV) E protein that the cytoplasmic tail contains Golgi targeting information (9). IBV M contains Golgi targeting information in its first transmembrane domain (57), while the transmembrane domains and cytoplasmic tail of mouse hepatitis virus (MHV) M appear to play a role in Golgi targeting (1, 36). Some coronavirus S proteins contain targeting information in their cytoplasmic tails; however, some do not (38, 39, 52, 63). Since S proteins can escape to the cell surface when highly expressed, S may rely on lateral interactions with other viral envelope proteins to localize to the budding site and be incorporated into newly assembling virions.

In line with its role in virus assembly, M is necessary for virus-like particle (VLP) formation (3, 10, 26, 40, 55, 59). M has been shown to interact with itself to form homo-oligomers (12). In addition, M interacts with E, S, and the viral nucleocapsid and is essential for virion assembly (reviewed in reference 21). Lateral interactions between the coronavirus envelope proteins are critical for efficient virus assembly. The interaction of S and M has been studied for MHV, and the cytoplasmic tail of each protein is important for interaction (16, 44). Specifically, deletion of an amphipathic region in the MHV M cytoplasmic tail abrogates efficient interaction with

* Corresponding author. Mailing address: Department of Cell Biology, The Johns Hopkins University School of Medicine, 725 N. Wolfe St., Baltimore, MD 21205. Phone: (410) 955-1809. Fax: (410) 955-4129. E-mail: machamer@jhmi.edu.

▽ Published ahead of print on 9 December 2009.

MHV S (11). The S and M proteins of IBV, bovine coronavirus, feline infectious peritonitis virus, and SARS-CoV have been shown to interact; however, information about the specific regions that are important for interaction remains elusive (16, 22, 26, 42, 64). Due to the presence of several accessory proteins in the virion envelope (23–25, 28, 51, 53), it is possible that the requirements for SARS-CoV S and M interaction could be different from those of previously studied coronaviruses.

In earlier work, we reported that SARS-CoV M retains SARS-CoV S intracellularly at the Golgi region when both proteins are expressed exogenously (39). We also demonstrated that the SARS-CoV S cytoplasmic tail interacts with *in vitro*-transcribed and -translated SARS-CoV M (39). Here, we show that the SARS-CoV M cytoplasmic tail is necessary for specific retention of SARS-CoV S at the Golgi region. We found a critical tyrosine residue at position 195 to be important for retaining SARS-CoV S Golgi membranes when coexpressed with M. When Y_{195} was mutated to alanine, the mutant protein, M_{Y195A}, did not reduce the amount of SARS-CoV S at the plasma membrane or reduce the extent of S carbohydrate processing as well as wild-type SARS-CoV M does. Additionally, mutation of Y_{195} in SARS-CoV M disrupted the S-M interaction *in vitro*. Thus, Y_{195} is likely to play a critical role in the assembly of infectious SARS-CoV.

MATERIALS AND METHODS

Plasmid construction. pCAGGS/SARS-CoV M and pCAGGS/SARS-CoV S were previously described (39). QuikChange (Stratagene, La Jolla, CA) site-directed mutagenesis was used to introduce deletions in pcDNA3.1/SARS-CoV M (39), using primers that flanked the deleted regions, according to the manufacturer's protocol. The amino acids indicated were deleted or mutated for the following constructs: $M_{\Delta1}$ (Y_{177}-T_{207}), $M_{\Delta2}$ (L_{137}-T_{207}), $M_{\Delta1a}$ (L_{205}-D_{214}), $M_{\Delta1b}$ (Y_{195}-K_{204}), $M_{\Delta1c}$ (R_{185}-A_{194}), $M_{\Delta bc}$ (S_{191}-R_{199}), M_{S190A}, M_{G191A}, M_{F192A}, M_{A193V}, M_{Y195A}, M_{R197A}, M_{Y198A}, and M_{Y203}. pcDNA3.1/SARS-CoV M_{Y195A} was created using primers that changed the nucleotides coding for SARS-CoV M Y_{195} to A_{195} according to the manufacturer's protocol. The sequenced deletions and mutations were then subcloned into the mammalian expression vector pCAGGS-MCS (43) (a kind gift from P. Bates) to increase expression levels using KpnI and XhoI sites. cDNA encoding vesicular stomatitis virus (VSV) G was excised from pBS/G (9) using HindIII and XbaI sites and subcloned into pcDNA3.1 (Invitrogen, Grand Island, NY) to create pcDNA3.1/VSV G. To create pCAGGS/VSV G, cDNA encoding the VSV G luminal and transmembrane domains was excised from pcDNA3.1/VSV G using EcoRI and BamHI and cDNA encoding the VSV G cytoplasmic tail was excised from pBS/G_{CT} (9) using BamHI and XhoI; these fragments were then subcloned into pCAGGS-MCS. To create pCAGGS/SARS-CoV M-G_{tail}, the cDNA sequence encoding M_1-R_{100} of SARS-CoV M was amplified from pcDNA3.1/SARS-CoV M by PCR flanked by KpnI and BamHI sites and the cDNA sequence encoding the cytoplasmic tail of VSV G (200 bp) was excised from pBS/G_{CT} using BamHI and XhoI; these fragments were then subcloned into pCAGGS-MCS using KpnI and XhoI.

Cells and culture. HeLa cells and HEK293T cells were maintained in Dulbecco's modified Eagle's medium (DMEM) (Invitrogen/Gibco, Grand Island, NY) supplemented with 10% fetal bovine serum (FBS) (Atlanta Biologicals, Lawrenceville, GA) and 0.1 mg/ml Normocin (InvivoGen, San Diego, CA) at 37°C and 5% CO_2.

Transient transfections. Fugene6 (Roche, Indianapolis, IN) was used to transfect each cDNA into cells according to the manufacturer's instructions. One day after plating of cells, 50% confluent HeLa or HEK293T cells were transfected with a total of 2 μg of DNA. When SARS-CoV S was coexpressed with SARS-CoV M or any M mutant, there was a decrease in the SARS-CoV S expression level. To counteract this decrease in S expression, we transfected S and M at a 3:1 ratio (1.5 μg pCAGGS/SARS-CoV S and 0.5 μg pCAGGS/SARS-CoV M, M mutant, or empty vector). In cases where SARS-CoV S was expressed alone, the remaining concentration of DNA was composed of empty pCAGGS vector. Fugene6 was first diluted in Opti-MEM (Invitrogen/Gibco, Grand Island, NY) before plasmid DNA was added at a 3:1 Fugene6:DNA ratio according to the manufacturer's instructions. The localization of SARS-CoV S and M was similar in HeLa and HEK293T cells; however, HeLa cells are flatter and easier to image and were thus used for indirect immunofluorescence microscopy, while 293T cells were used for the biochemical experiments because the transfection efficiency was higher. All mutants were tested by indirect immunofluorescence in HEK293T cells and behaved identically as in HeLa cells.

Antibodies. Rabbit anti-SARS-CoV S and rabbit anti-SARS-CoV M polyclonal antibodies were previously described (39). Mouse monoclonal SARS-CoV S antibodies were from Biodefense and Emerging Infections Research (BEI) Resources (Manassas, VA). The hybridoma line for mouse anti-VSV G monoclonal antibody I1 was grown as described previously (35). Rabbit anti-VSV G polyclonal antibody (61) and rabbit anti-golgin-160 antibody (19) were previously described. Mouse anti-GM130 antibody was from BD Biosciences (San Diego, CA). Alexa 488-conjugated donkey anti-mouse IgG was from Invitrogen/Molecular Probes (Eugene, OR). Texas red-conjugated donkey anti-rabbit IgG was from Jackson ImmunoResearch (Westgrove, PA). Horseradish peroxidase (HRP)-conjugated anti-rabbit IgG was from Amersham/GE Healthcare (Piscataway, NJ).

Indirect immunofluorescence microscopy. At 24 h posttransfection, HeLa cells were washed in phosphate-buffered saline (PBS) and fixed for 10 min in 3% paraformaldehyde in PBS. Fixative was quenched in PBS containing 10 mM glycine (PBS-gly). Cells were permeabilized for 3 min in 0.5% Triton X-100 in PBS-gly and then stained for 20 min with primary antibodies diluted in 1% bovine serum albumin (BSA) in PBS-gly. The following combinations were used: rabbit anti-SARS-CoV M (1:400) and mouse anti-GM130 (1:200), rabbit anti-SARS-CoV M (1:400) and mouse anti-SARS-CoV S (1:25), affinity-purified rabbit anti-VSV G (1:25) and mouse anti-GM130 (1:200), affinity-purified rabbit anti-VSV G (1:25) and mouse anti-SARS-CoV S (1:25), mouse anti-VSV G hybridoma tissue culture supernatant (undiluted) and rabbit anti-golgin-160 (1:200), and mouse anti-VSV G hybridoma tissue culture supernatant (undiluted) and rabbit anti-SARS-CoV M (1:400). Cells were then stained for 20 min with secondary antibodies in the following combination: Alexa 488-conjugated donkey anti-mouse IgG (1:500) and Texas red-conjugated donkey anti-rabbit IgG (1:400). Cells were washed twice with PBS-gly after each step for a total of 5 min and mounted in glycerol containing 0.1 M *N*-propylgallate. Images were obtained with a Axioscop microscope (Zeiss, Thornwood, NJ) equipped for epifluorescence using a Sensys charge-coupled-device camera (Photometrics, Tucson, AZ) and IP Lab software (Scanalytics, Vienna, VA).

Cell surface biotinylation. For biotinylation experiments, HEK293T cells were seeded on poly-L-lysine-treated (1 mg/ml) tissue culture dishes to increase cell adherence. At 24 h posttransfection, HEK293T cells were washed twice in PBS. Cells were incubated for 30 min on ice with 1 mg/ml biotin (EZ-Link Sulfo-NHS-LC-Biotin; Pierce/ThermoScientific, Rockford, IL) in PBS. Cells were washed twice and then incubated for 3 min in PBS containing 50 mM glycine to quench the biotin. Cells were lysed in biotinylation lysis buffer (10 mM HEPES [pH 7.2], 0.2% NP-40, 150 mM NaCl) containing protease inhibitor cocktail (Sigma, St. Louis, MO) at 0°C for 10 min. Lysates were clarified at 16,000 × g for 10 min at 4°C. Ten percent of the lysate was removed for quantifying total S. The remainder of the lysate was added to 75 μl of washed streptavidin agarose resin (Pierce/ThermoScientific, Rockford, IL) to bind biotinylated proteins overnight at 4°C with rotation. Streptavidin beads were washed 3 times in lysis buffer, and biotinylated proteins were eluted at 100°C in 1× sample buffer (50 mM Tris-HCl [pH 6.8], 2% sodium dodecyl sulfate [SDS], 20% glycerol, 0.025% bromophenol blue) and 5% 2-mercaptoethanol. Samples were subjected to 8% SDS–polyacrylamide gel electrophoresis (PAGE) and transferred to polyvinylidene difluoride membrane (PVDF) (Millipore, Bedford, MA) for Western blotting. Membranes were blocked for 30 min in 5% nonfat dry milk made in Tris-buffered saline containing Tween (TBST) (150 mM NaCl, 10 mM Tris-HCl [pH 7.4], 0.05% Tween 20) and then washed three times in TBST. Membranes were incubated overnight at 4°C in primary rabbit anti-SARS-CoV S polyclonal antibody diluted 1:5,000 in 3% BSA and 0.02% NaN_3 in TBST. Membranes were washed three times in TBST and then incubated for 1 h in HRP-conjugated anti-rabbit IgG diluted 1:10,000 in 5% nonfat dry milk made in TBST. Membranes were washed three times in TBST and then treated with HyGlo chemiluminescence reagent (Denville Scientific, Metuchen, NJ) according to the manufacturer's instructions. Membranes were analyzed using a Versa Doc imaging station (Bio-Rad, Hercules, CA) and quantified using Quantity One software (Bio-Rad).

Metabolic labeling/endo H digestion. At 24 h posttransfection, HEK293T cells were pulse-labeled and chased as described previously (39). Briefly, HEK293T cells were starved in methionine- and cysteine-free DMEM for 20 min, labeled

for 20 min with 50 μCi of Expre^{35}S^{35}S (Perkin Elmer, Waltham, MA) [^{35}S]methionine-cysteine per dish in methionine- and cysteine-free DMEM, and then chased for various times in DMEM/10% FBS. Cells were washed in PBS and then lysed in detergent solution (50 mM Tris-HCl [pH 8.0], 1% NP-40, 0.4% deoxycholate [DOC], 62.5 mM EDTA) containing protease inhibitor cocktail. Lysates were clarified, SDS was added to a final concentration of 0.2%, and SARS-CoV S proteins were immunoprecipitated with rabbit-anti-SARS-CoV S polyclonal antibodies overnight at 4°C. Immune complexes were collected with washed *Staphylococcus aureus* Pansorbin cells (Calbiochem, San Diego, CA) and washed 3 times in radioimmunoprecipitation assay (RIPA) buffer (0.1% SDS, 50 mM Tris-HCl [pH 8.0], 1% DOC, 150 mM NaCl, 1% Triton X-100). Samples were eluted in 1% SDS in 50 mM Tris (pH 6.8) at 100°C and digested with 0.1 mU/μl endoglycosidase H (endo H) (New England Biolabs, Beverly, MA) in 150 mM sodium citrate [pH 5.5] overnight at 37°C. Concentrated sample buffer was added to 1×, and samples were subjected to 8% SDS–PAGE. Labeled proteins were visualized by using a Molecular Imager FX phosphorimager (Bio-Rad) and quantified using Quantity One software.

Sequence alignment. A sequence alignment of M cytoplasmic tail amino acids was generated using MultAlin software (8; http://bioinfo.genotoul.fr/multalin/). The GenBank nucleotide sequence accession numbers of the M proteins aligned are as follows: IBV M, NP_040835.1; MHV M, NP_045301.1; BCV M, AAK29779.2; HCV OC43 M, NP_937953.1; HCV HKU1 M, YP_173241.1; SARS-CoV M, NP_828855.1; HCV NL63 M, YP_003770.1; HCV 229E M, NP_073555.1; FIPV M, YP_239357.1; and TGEV M, ABF72147.1. The full-length M sequences were used; however, only the relevant portion of the alignment is shown (see Fig. 7).

IVTT. Recombinant C-terminally His-tagged full-length SARS-CoV S expressed with baculovirus and purified from Sf9 insect cells was obtained from BEI Resources. Full-length radiolabeled SARS-CoV M and M_{Y195A} were translated *in vitro* using the TNT quick coupled transcription/translation system (Promega Corporation, Madison, WI). Briefly, pcDNA3.1/SARS-CoV M or pcDNA3.1/SARS-CoV M_{Y195A} was incubated with TNT master mix in the presence of Easy Tag [^{35}S]methionine (Perkin Elmer) and canine pancreatic microsomal membranes (Promega Corporation, Madison, WI) for 90 min at 30°C. *In vitro*-transcribed and -translated proteins were solubilized in *in vitro* transcription and translation (IVTT) binding buffer (50 mM HEPES [pH 7.1], 100 mM NaCl, 10 mM EDTA, 5 mM $MgCl_2$, 1 mM dithiothreitol [DTT], 0.1% NP-40). Equal amounts of the IVTT reaction mixtures (with SARS-CoV M or M_{Y195A}) were added to full-length His-tagged SARS-CoV S tail prebound to Ni-nitrilotriacetic acid (NTA)-agarose or Ni-NTA-agarose alone and incubated with rotation at room temperature for 1 h. Bound proteins were washed in IVTT binding buffer, eluted in sample buffer, and subjected to 15% SDS–PAGE. Gels were stained with Coomassie blue to ensure equal S protein load, and labeled proteins were visualized by using a Molecular Imager FX phosphorimager and quantified using Quantity One software.

RESULTS

The cytoplasmic tail of SARS-CoV M specifically retains SARS-CoV S in the Golgi complex. We have shown that SARS-CoV S localizes to the plasma membrane when exogenously expressed alone in cells. However, when SARS-CoV S is coexpressed with SARS-CoV M, S is retained intracellularly at the Golgi complex near the virus assembly site (39). This phenomenon has also been demonstrated for the S and M proteins of several other coronaviruses (42, 44). To determine if the ability of M to retain S was specific, we coexpressed SARS-CoV M with the VSV glycoprotein (VSV G). VSV G is a well-studied viral glycoprotein that traffics quickly through the secretory pathway, localizes to the plasma membrane at steady state (38), and has no homology with SARS-CoV M. When coexpressed with VSV G, SARS-CoV M did not retain VSV G intracellularly at the Golgi complex (Fig. 1B). This suggests that the ability of the SARS-CoV M tail to retain SARS-CoV S is specific.

It has been shown that SARS-CoV S and M can interact *in vitro* and *in vivo* (22, 26, 39); however, the specific requirements for S-M interaction have not been determined. Published data for MHV implicate the cytoplasmic tail of each protein in the S and M interaction, although the specific region important for SARS-CoV S-M interaction has not been demonstrated (16, 44). To determine if the region of SARS-CoV M necessary for interaction with S was limited to the cytoplasmic tail, we created a chimeric protein (SARS-CoV M-G_{tail}) consisting of the SARS-CoV M luminal and transmembrane domains (M_1-R_{100}) fused to the cytoplasmic tail of VSV G. The chimeric protein SARS-CoV M-G_{tail} was localized to the Golgi complex when exogenously expressed in HeLa cells (Fig. 1C). This was expected since the SARS-CoV M transmembrane domains are important for Golgi localization (unpublished data) (60). However, unlike full-length M, M-G_{tail} did not retain SARS-CoV S intracellularly at the Golgi complex when the two proteins were coexpressed, suggesting that the SARS-CoV M cytoplasmic tail was necessary to retain SARS-CoV S in the Golgi region of transfected cells (Fig. 1C). A reciprocal chimera was also made, consisting of the VSV G luminal and transmembrane domains fused to the cytoplasmic tail of SARS-CoV M. The resulting chimera, VSV G-M_{tail}, was found to be mislocalized with both ER and Golgi staining (data not shown). However, when coexpressed with SARS-CoV S, VSV G-M_{tail} was able to retain S intracellularly, again indicating that the SARS-CoV M cytoplasmic tail was necessary to retain SARS-CoV S in the Golgi region (data not shown).

Mapping the S-M interaction site in the SARS-CoV M cytoplasmic tail. To map the interaction between the SARS-CoV S and M proteins, we made deletions of 120, 70, or 30 amino acids in the SARS-CoV M cytoplasmic tail near the C terminus. The M protein lacking 120 amino acids was unstable and was therefore not included in the subsequent analysis. The mutant protein SARS-CoV $M_{\Delta1}$ lacks 30 amino acids (Y_{177}-T_{207}) of the M cytoplasmic tail. The mutant protein SARS-CoV $M_{\Delta2}$ lacks 70 amino acids (L_{137}-T_{207}) of the M cytoplasmic tail (Fig. 2). Our rabbit anti-SARS-CoV M antibody recognizes the extreme 15 C-terminal amino acids, so these residues were not deleted in either mutant.

To determine if SARS-CoV $M_{\Delta1}$ and SARS-CoV $M_{\Delta2}$ were correctly targeted to the Golgi compartment, the mutant proteins were transiently expressed and analyzed by indirect immunofluorescence microscopy. At 24 h posttransfection, cells were fixed, permeabilized, and stained with antibodies to SARS-CoV M and the Golgi marker GM130. Similar to wild-type SARS-CoV M, both $M_{\Delta1}$ and $M_{\Delta2}$ localized to the Golgi region (Fig. 3A).

Since the results of our immunofluorescence experiments suggested that SARS-CoV S and M interact in transfected cells, we used this assay to determine if SARS-CoV $M_{\Delta1}$ and SARS-CoV $M_{\Delta2}$ could interact with and retain SARS-CoV S intracellularly at the Golgi complex. HeLa cells transiently expressing SARS-CoV S with SARS-CoV M, SARS-CoV $M_{\Delta1}$, or SARS-CoV $M_{\Delta2}$ were fixed, permeabilized, and stained with antibodies to SARS-CoV S and SARS-CoV M. As shown earlier, when SARS-CoV S was expressed alone, it was present at the cell surface. Unlike full-length SARS-CoV M, neither SARS-CoV $M_{\Delta1}$ nor SARS-CoV $M_{\Delta2}$ retained SARS-CoV S in Golgi membranes, and S accumulated at the plasma membrane similarly to its accumulation when it was expressed alone (Fig. 3B).

To quantify the steady-state level of SARS-CoV S at the

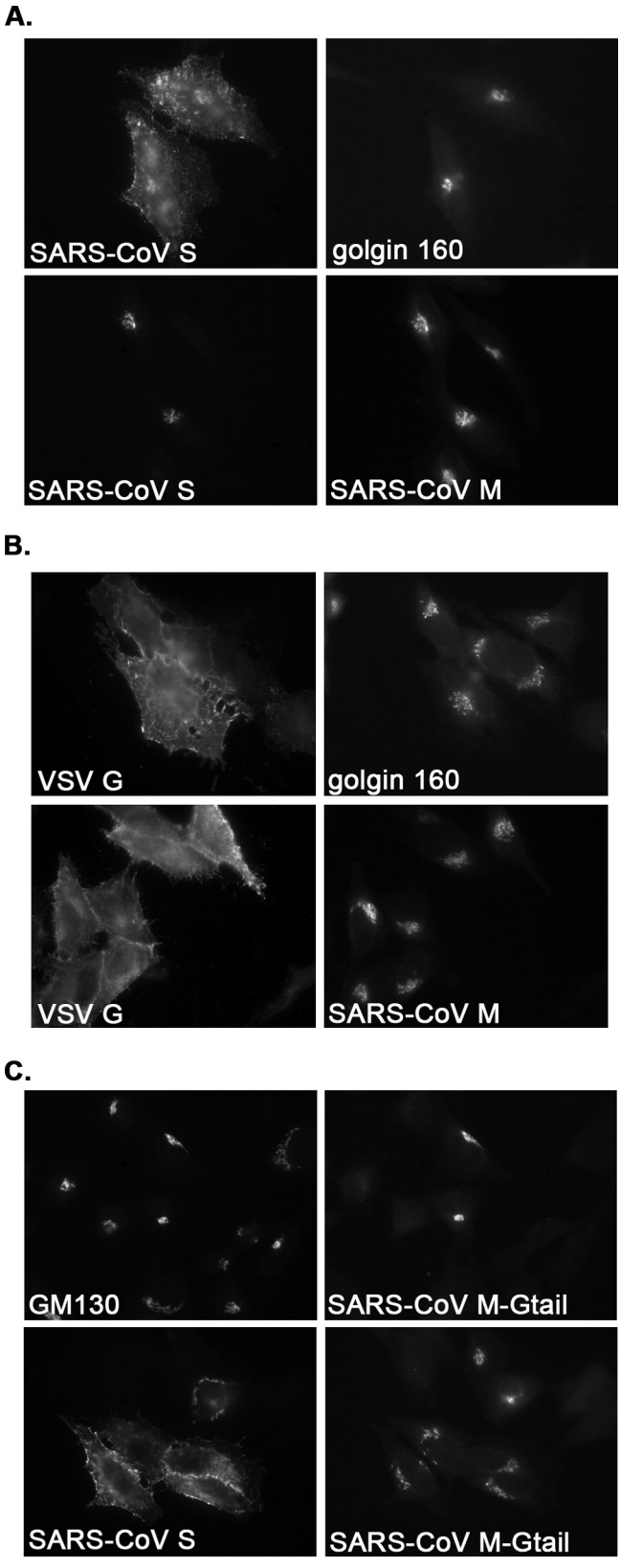

FIG. 1. The cytoplasmic tail of SARS-CoV M specifically mediates interaction with SARS-CoV S. HeLa cells expressing SARS-CoV S in the presence or absence of SARS-CoV M (A), SARS-CoV M in the presence or absence of VSV G (B), or SARS-CoV M-G_{tail} in the presence or absence of SARS CoV-S (C) for 24 h were fixed, permeabilized, and stained with mouse anti-SARS-CoV S and rabbit anti-golgin-160 (a Golgi marker) or rabbit anti-SARS-CoV M (A), mouse anti-VSV G and rabbit anti-golgin-160 or rabbit anti-SARS-CoV M (B), or rabbit anti-VSV G and mouse anti-GM130 (a Golgi marker) or mouse anti-SARS-CoV S (C). The secondary antibodies were Alexa 488-conjugated donkey anti-mouse IgG and Texas red-conjugated donkey anti-rabbit IgG. The same field is shown for each horizontal set of panels.

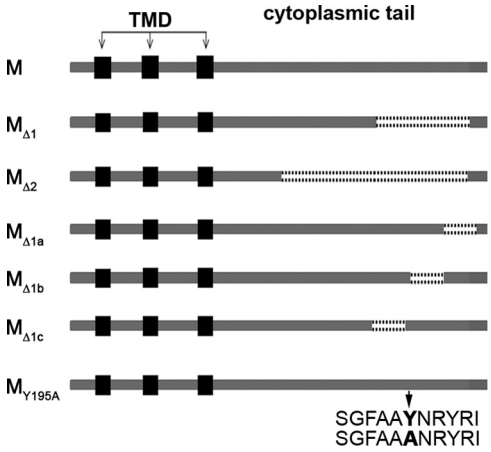

FIG. 2. Cartoon depicting wild-type SARS-CoV M and M mutants. Deletions or point mutations were introduced into the cytoplasmic tail of SARS-CoV M using site-directed mutagenesis. Deleted regions are marked with dotted lines. The Y_{195} mutation is in bold and marked with a black arrow in the sequence alignment below the cartoon. Gray arrows show transmembrane domains (TMD).

plasma membrane, we performed a cell surface biotinylation assay. We used HEK293T cells for this and other biochemical assays due to their higher transfection efficiency. All mutants were tested by indirect immunofluorescence in HEK293T cells and behaved identically to HeLa cells. HEK293T cells expressing SARS-CoV S with SARS-CoV M, SARS-CoV $M_{\Delta1}$, SARS-CoV $M_{\Delta2}$, or empty vector were biotinylated at 0°C with a non-membrane-permeating biotinylating reagent. Biotinylated S proteins were isolated with streptavidin agarose resin and analyzed by SDS-PAGE and Western blotting with antibodies to SARS-CoV S (Fig. 3C). The total amount of S protein in the sample was determined by running 10% of the lysate. Total S protein, as well as biotinylated surface S protein, was quantified and normalized to the amount of SARS-CoV S coexpressed with empty vector. When SARS-CoV S was coexpressed with wild-type SARS-CoV M for 24 h, we observed a 60% reduction in the amount of SARS-CoV S present at the plasma membrane (Fig. 3D). However, coexpression with either SARS-CoV $M_{\Delta1}$ or SARS-CoV $M_{\Delta2}$ did not reduce the amount of SARS-CoV S present on the cell surface (Fig. 3D).

SARS-CoV S is trafficked through the secretory pathway when expressed alone and accumulates at the plasma membrane (4, 20, 39, 52, 54, 56). Since SARS-CoV M but not $M_{\Delta1}$ or $M_{\Delta2}$ retained S intracellularly at the Golgi compartment and reduced the amount of S present at the plasma membrane (Fig. 3), we next analyzed S protein trafficking through the

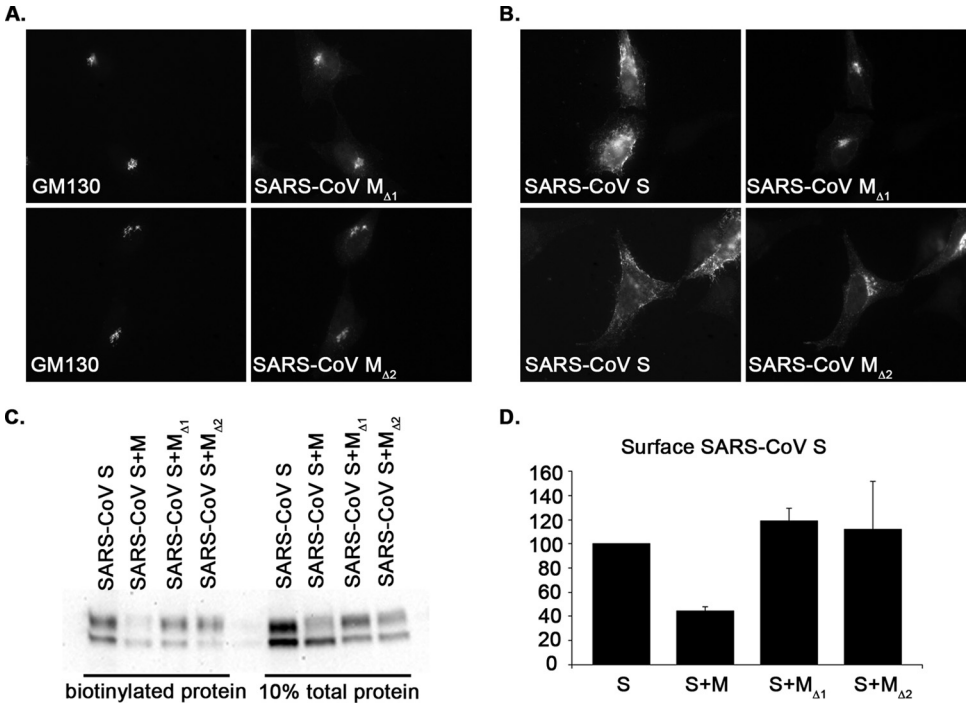

FIG. 3. SARS-CoV $M_{\Delta1}$ and $M_{\Delta2}$ localize to the Golgi compartment but do not retain SARS-CoV S or reduce the amount of SARS-CoV S at the plasma membrane. (A) HeLa cells expressing SARS-CoV $M_{\Delta1}$ or SARS-CoV $M_{\Delta2}$ for 24 h were fixed, permeabilized, and stained with rabbit anti-SARS-CoV M and mouse anti-GM130. Secondary antibodies were Alexa 488-conjugated donkey anti-mouse IgG and Texas red-conjugated donkey anti-rabbit IgG. The same field is shown for each horizontal set of panels. (B) HeLa cells coexpressing SARS-CoV S and $M_{\Delta1}$ or $M_{\Delta2}$ for 24 h were fixed, permeabilized, and stained with mouse anti-SARS-CoV S and rabbit anti-SARS-CoV M. Secondary antibodies were Alexa 488-conjugated donkey anti-mouse IgG and Texas red-conjugated donkey anti-rabbit IgG. The same field is shown for each horizontal set of panels. (C and D) HEK293T cells expressing SARS-CoV S in the absence or presence of SARS-CoV M, $M_{\Delta1}$, or $M_{\Delta2}$ were surface biotinylated at 24 h posttransfection. After lysis, 10% of the lysate was saved for quantification of total S. Biotinylated proteins were collected from the remainder of the lysate by using streptavidin agarose resin, washed, and eluted in sample buffer. After SDS-PAGE and Western blotting with antibodies to SARS-CoV S (C), total biotinylated S protein was quantified for each sample (D). Values in panel D are normalized to the amount of biotinylated S when expressed alone. The averages of the results of three independent experiments ± standard errors of the means are shown.

secretory pathway when coexpressed with the M mutants. As a glycoprotein moves through the secretory pathway, its sugars are modified (18); in the medial Golgi complex, N-linked sugars become resistant to digestion with endoglycosidase H (endo H). The rate and extent of glycoprotein trafficking through the secretory pathway en route to the plasma membrane can be inferred from the amount of endo H-resistant protein over time after pulse-labeling. HEK293T cells exogenously expressing SARS-CoV S and SARS-CoV M or empty vector were pulse-labeled with [^{35}S]methionine-cysteine and chased for various times. S protein was immunoprecipitated, denatured, and digested with endo H. When SARS-CoV S was expressed alone, approximately 70% of labeled SARS-CoV S was resistant to digestion with endo H after 40 min of chase. However, when SARS-CoV S was coexpressed with SARS-CoV M, only 25% of SARS-CoV S was resistant to endo H digestion after 40 min of chase, indicating that the majority of labeled S had not reached the medial Golgi compartment (Fig. 4). Coexpression with SARS-CoV $M_{\Delta1}$ or $M_{\Delta2}$ had little effect on the amount of SARS-CoV S carbohydrate processing. This suggests that wild-type M but not $M_{\Delta1}$ or $M_{\Delta2}$ retains S predominantly in a pre-medial Golgi compartment. Given that SARS-CoV $M_{\Delta1}$ and SARS-CoV $M_{\Delta2}$ had similar phenotypes when coexpressed with SARS-CoV S, we concluded that the 30 amino acids near the C terminus were important for S and M interaction, since this region was missing from both SARS-CoV $M_{\Delta1}$ and $M_{\Delta2}$.

Finer mapping of the S-M interaction site in the SARS-CoV M cytoplasmic tail. To further map the SARS-CoV S and M interaction, we made smaller deletions in and surrounding the region deleted from SARS-CoV $M_{\Delta1}$ (Fig. 2). SARS-CoV $M_{\Delta1a}$, SARS-CoV $M_{\Delta1b}$, and SARS-CoV $M_{\Delta1c}$ were missing amino acids L_{205}-D_{214}, Y_{195}-K_{204}, or R_{185}-A_{194}, respectively. When exogenously expressed for 24 h in HeLa cells, SARS-CoV $M_{\Delta1a}$, $M_{\Delta1b}$, and $M_{\Delta1c}$ all localized to the Golgi region (Fig. 5A). However, when coexpressed with SARS-CoV S, only SARS-CoV $M_{\Delta1a}$ retained S intracellularly at the Golgi region (Fig. 5B). When SARS-CoV $M_{\Delta1b}$ and $M_{\Delta1c}$ were coexpressed with SARS-CoV S, S was present on the plasma membrane at steady state (Fig. 5B).

To quantify the amount of SARS-CoV S at the plasma membrane, we performed a cell surface biotinylation assay as described above. Coexpression with SARS-CoV $M_{\Delta1a}$ reduced the amount of SARS-CoV S present at the plasma membrane by approximately 60%, similar to coexpression with wild-type SARS-CoV M (Fig. 5D and 3D). However, coexpression with SARS-CoV $M_{\Delta1b}$ or SARS-CoV $M_{\Delta1c}$ did not reduce the amount of SARS-CoV S present at the cell surface.

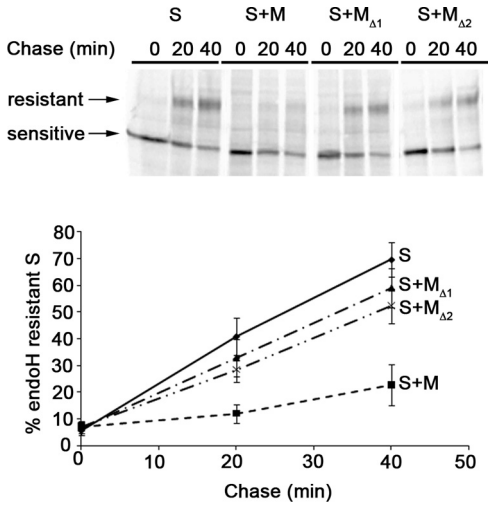

FIG. 4. SARS-CoV $M_{\Delta1}$ and $M_{\Delta2}$ are less effective at reducing SARS-CoV S trafficking through the Golgi compartment than wild-type SARS-CoV M. At 24 h posttransfection, HEK293T cells expressing SARS-CoV S in the absence or presence of SARS-CoV M, $M_{\Delta1}$, or $M_{\Delta2}$ were labeled with [^{35}S]methionine-cysteine for 20 min and then chased for 0, 20, or 40 min. After lysis, S proteins were immunoprecipitated, denatured, and digested with endo H. Endo H-sensitive and -resistant forms are indicated. After electrophoresis and phosphorimaging, the percentage of endo H-resistant S was quantified. The averages of the results of five independent experiments ± standard errors of the means are shown.

To determine if SARS-CoV $M_{\Delta1a}$, $M_{\Delta1b}$, or $M_{\Delta1c}$ could reduce the extent of SARS-CoV S carbohydrate processing, we performed a pulse-chase endo H-trafficking assay as described above. After 40 min of chase, approximately 70% of radiolabeled SARS-CoV S had moved to the medial Golgi compartment and was resistant to endo H digestion. When SARS-CoV S was coexpressed with SARS-CoV $M_{\Delta1a}$, only 25% was resistant to digestion with endo H after 40 min of chase (Fig. 6), which was similar to the result when S was coexpressed with wild-type M (Fig. 4). This suggests that $M_{\Delta1a}$ was able to retain S in a pre-medial Golgi compartment. However, when SARS-CoV $M_{\Delta1b}$ or $M_{\Delta1c}$ was coexpressed with SARS-CoV S, the extent of S carbohydrate processing was not reduced (Fig. 6) and was similar to the amount of carbohydrate processing when S was coexpressed with SARS-CoV $M_{\Delta1}$ (Fig. 4). Thus, neither $M_{\Delta1b}$ nor $M_{\Delta1c}$ was able to retain S in a pre-medial Golgi compartment. When SARS-CoV S was coexpressed with SARS-CoV $M_{\Delta1}$, SARS-CoV $M_{\Delta1b}$, or SARS-CoV $M_{\Delta1c}$, the amount of SARS-CoV S that was resistant to endo H digestion after 40 min of chase was less than the amount of endo H-resistant S after 40 min of chase when S was expressed alone (Fig. 4). Thus, it is possible that some residual interaction of S with the mutant M proteins still exists. The implications of this observation will be discussed below.

Tyrosine 195 is important for SARS-CoV S-M interaction. Since neither SARS-CoV $M_{\Delta1b}$ nor $M_{\Delta1c}$ retained SARS-CoV S intracellularly at the Golgi and they do not contain overlapping deleted amino acids, we concluded that the S interaction site was near the shared border between the two deleted regions. To test this, we created another deletion mutant, SARS-CoV $M_{\Delta bc}$, which is missing 5 amino acids from both $M_{\Delta1b}$ and $M_{\Delta1c}$ (S_{191}-R_{199}), spanning the $M_{\Delta1b}$/$M_{\Delta1c}$ junction. SARS-CoV $M_{\Delta bc}$ was unable to retain SARS-CoV S intracellularly as assayed by immunofluorescence microscopy, surface biotinylation, or pulse-chase (data not shown), and it behaved similarly to $M_{\Delta1}$, $M_{\Delta2}$, $M_{\Delta1b}$, and $M_{\Delta1c}$. Sequence alignment of various coronavirus M protein cytoplasmic tails revealed the presence of several conserved residues spanning the SARS-CoV $M_{\Delta1b}$ and $M_{\Delta1c}$ junction (Fig. 7). To determine if the conserved amino acids were important for SARS-CoV S and M interaction, we mutated them individually to alanine or valine (M_{S190A}, M_{G191A}, M_{F192A}, M_{A193V}, M_{Y195A}, M_{R197A}, M_{Y198A}, or M_{Y203}) (data not shown). Only one mutant, SARS-CoV M_{Y195A}, was unable to retain SARS-CoV S intracellularly. When analyzed by indirect immunofluorescence microscopy, SARS-CoV M_{Y195A} was localized to the Golgi region but did not retain SARS-CoV S intracellularly (Fig. 8A). Unlike wild-type M, coexpression of SARS-CoV M_{Y195A} did not reduce the amount of SARS-CoV S present on the plasma membrane as measured by surface biotinylation (Fig. 8B). In addition, SARS-CoV M_{Y195A} behaved similarly to $M_{\Delta1}$ when SARS-CoV S carbohydrate processing was measured by endo H resistance after pulse-chase (Fig. 8C). Thus, we conclude that disruption of Y_{195} was responsible for the inability of SARS-CoV $M_{\Delta1}$, $M_{\Delta2}$, $M_{\Delta1b}$, and $M_{\Delta1c}$ to interact with SARS-CoV S. Although Y_{195} is present in $M_{\Delta1c}$, the context in which it is presented is probably changed, since it is the first amino acid after the deletion.

Interaction of SARS-CoV S with M *in vitro* is disrupted by mutating Y_{195}. Our previously published results suggest that SARS-CoV S and M interact directly (39). To determine if the Y_{195A} mutation disrupts SARS-CoV S and M interaction *in vitro*, we performed a binding assay using *in vitro*-transcribed and -translated SARS-CoV M or M_{Y195A} incubated with full-length His-tagged SARS-CoV S. The solubilized *in vitro*-transcribed and -translated M proteins were incubated with His-tagged SARS-CoV S prebound to nickel beads or with nickel beads alone. Samples were analyzed by SDS-PAGE and phosphorimaging. *In vitro*-transcribed and -translated SARS-CoV M bound specifically to His-tagged SARS-CoV S (Fig. 9). However, when Y_{195} was mutated to alanine, the amount of SARS-CoV M_{Y195A} binding to His-tagged SARS-CoV S was reduced to background levels (Fig. 9). We were unable to detect *in vitro* binding when only the soluble, recombinant tail of each protein was examined, suggesting that transmembrane regions of each may be important for orienting the tails (data not shown).

Taken together, our results suggest that the SARS-CoV S and M interaction is mediated by the cytoplasmic tail of SARS-CoV M and that a single residue, Y_{195}, is necessary for efficient S and M interaction.

DISCUSSION

Unlike many well-studied enveloped viruses, coronaviruses assemble intracellularly at the ERGIC (reviewed in reference 21). Thus, the proteins in the virion envelope must be targeted to the ERGIC for assembly. As for most other enveloped viruses, lateral interactions between coronavirus envelope proteins are important for the proper assembly of infectious virus. The coronavirus M protein was originally thought to determine

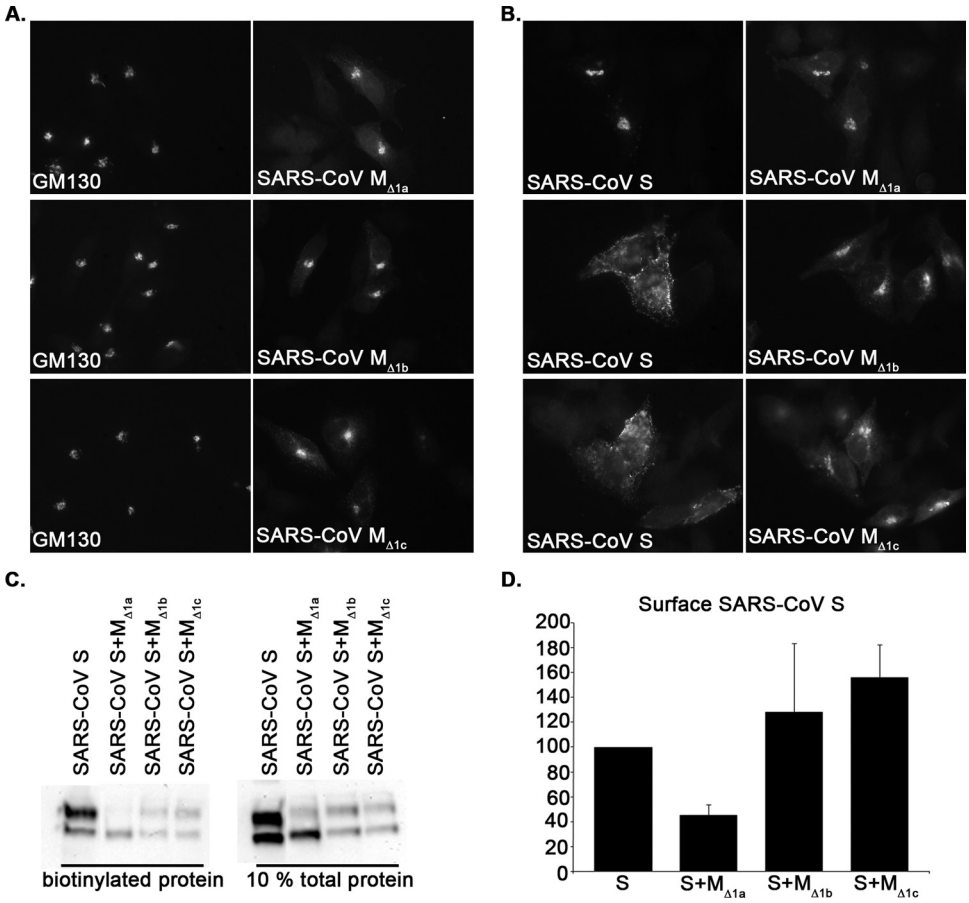

FIG. 5. SARS-CoV $M_{\Delta 1a}$, $M_{\Delta 1b}$, and $M_{\Delta 1c}$ localize to the Golgi compartment, but only SARS-CoV $M_{\Delta 1a}$ can retain SARS-CoV S and reduce the amount of SARS-CoV S at the plasma membrane. (A) HeLa cells expressing SARS-CoV $M_{\Delta 1a}$, $M_{\Delta 1b}$, or $M_{\Delta 1c}$ for 24 h were fixed, permeabilized, and stained with rabbit anti-SARS-CoV M and mouse anti-GM130. Secondary antibodies were Alexa 488-conjugated donkey anti-mouse IgG and Texas red-conjugated donkey anti-rabbit IgG. The same field is shown for each horizontal set of panels. (B) HeLa cells coexpressing SARS-CoV S and $M_{\Delta 1a}$, $M_{\Delta 1b}$, or $M_{\Delta 1c}$ for 24 h were fixed, permeabilized, and stained with mouse anti-SARS-CoV S and rabbit anti-SARS-CoV M. Secondary antibodies were Alexa 488-conjugated donkey anti-mouse IgG and Texas Red-conjugated donkey anti-rabbit IgG. The same field is shown for each horizontal set of panels. (C and D) HEK293T cells expressing SARS-CoV S in the absence or presence of SARS-CoV $M_{\Delta 1a}$, $M_{\Delta 1b}$, or $M_{\Delta 1c}$ were surface biotinylated. After lysis, biotinylated cell surface proteins were collected by using streptavidin agarose resin, washed, and eluted in sample buffer. After SDS-PAGE and Western blotting with rabbit anti-SARS-CoV S antibodies, total biotinylated S protein was quantified for each sample (D). Values in panel D are normalized to the amount of biotinylated S when expressed alone. The averages of the results of three independent experiments ± standard errors of the means are shown.

the location of virus assembly, since it can interact with the other viral structural proteins. However, since the M proteins of several coronaviruses localize past the budding site at steady state (29), it is thought that other factors, such as lateral interactions with other structural proteins, influence the location of the assembly site.

Previously, we determined that a dibasic ER retrieval signal found in the cytoplasmic tail of SARS-CoV S promoted interaction with the SARS-CoV M protein, presumably by increasing the possibilities for interaction during cycling (39). Here, we identified a critical tyrosine residue in the SARS-CoV M cytoplasmic tail that is necessary for efficient interaction with SARS-CoV S. When SARS-CoV S is expressed alone, it localizes to the plasma membrane, past the budding compartment. However, when SARS-CoV S is coexpressed with SARS-CoV M (39), M mediates intracellular retention of S in a pre-medial Golgi compartment near the virus assembly site. When coexpressed with SARS-CoV S, SARS-CoV M also reduced the amount of S present at the plasma membrane. Importantly, VSV G was not retained intracellularly by SARS-CoV M. This was expected, since coronavirus lateral interactions exclude host proteins from the assembling virion (12). Additionally, a chimeric protein consisting of the cytoplasmic tail of VSV G fused to the luminal and transmembrane domains of SARS-CoV M, M-G_{tail}, did not retain SARS-CoV S intracellularly. However, the reciprocal chimera consisting of the cytoplasmic tail of SARS-CoV M fused to the luminal and transmembrane domains of VSV G was able to retain SARS-CoV S intracellularly. These results suggest that the cytoplasmic tail of SARS-CoV M is necessary to mediate the SARS-CoV S-M interaction. This lateral S-M interaction is presumably how S is localized to the budding site and incorporated into newly assembled virions in infected cells.

We found that a critical tyrosine residue, Y_{195}, in the cytoplasmic tail of SARS-CoV M was important for retaining S at the Golgi complex. When Y_{195} was mutated to alanine, the

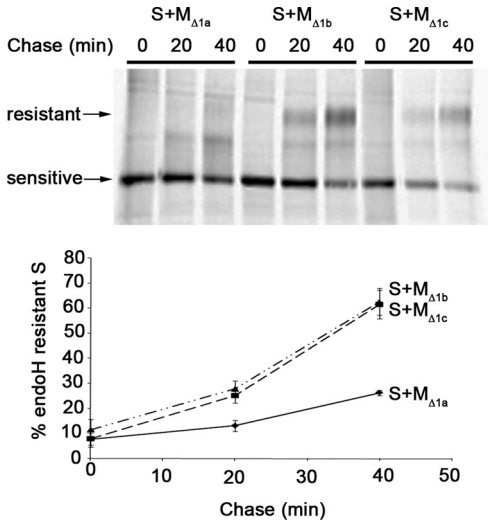

FIG. 6. Neither SARS-CoV $M_{\Delta 1b}$ nor $M_{\Delta 1c}$ slows SARS-CoV S trafficking through the Golgi compartment. HEK293T cells expressing SARS-CoV S in the presence of SARS-CoV $M_{\Delta 1a}$, $M_{\Delta 1b}$, or $M_{\Delta 1c}$ were labeled with [^{35}S]methionine-cysteine for 20 min and then chased for 0, 20, or 40 min. After lysis, S proteins were immunoprecipitated, denatured, and digested with endo H. Endo H-sensitive and -resistant forms are indicated. After electrophoresis and phosphorimaging, the percentage of endo H-resistant S was quantified. The averages of the results of three independent experiments ± standard errors of the means are shown.

mutant protein, SARS-CoV M_{Y195A}, did not retain S in the Golgi region when the two proteins were coexpressed. The expression of SARS-CoV M_{Y195A} did not reduce the amount of SARS-CoV S present at the plasma membrane or reduce S carbohydrate processing due to retention in a pre-medial Golgi compartment. Also, M_{Y195A} was unable to interact with SARS-CoV S *in vitro*. Importantly, M_{Y195A} was properly localized to the Golgi complex (Fig. 8A) and had a half-life similar to that of wild-type SARS-CoV M (data not shown). The importance of SARS-CoV M_{Y195} in S-M interaction was confirmed by using an *in vitro* binding assay. We do not believe that phosphorylation of Y_{195} is the basis for its importance in S-M interaction, since we have found no evidence that M is phosphorylated (unpublished data). Other tyrosine-based post-translation modifications, such as tyrosine nitration, are possible (27), but more work needs to be done to implicate or rule out tyrosine modifications as the basis for SARS-CoV S and M interaction. It is also possible that the critical tyrosine residue could be structurally important for S-M interaction. A well-known tyrosine-based protein-protein interaction motif is YXXΦ, where X is any amino acid and Φ is a bulky, hydro-

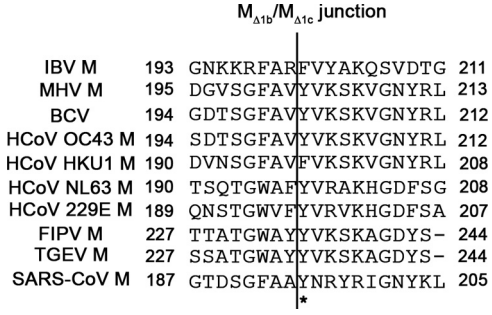

FIG. 7. Sequence alignment of CoV M protein cytoplasmic tails. The SARS-CoV $M_{\Delta 1b}/M_{\Delta 1c}$ junction is marked with a vertical line. Y_{195} that is mutated in SARS-CoV M_{Y195A} is marked with an asterisk. IBV, avian infectious bronchitis virus; MHV, mouse hepatitis virus; BCV, bovine coronavirus; HCoV, human coronavirus; FIPV, feline infectious peritonitis virus; TGEV, porcine transmissible gastroenteritis coronavirus; SARS-CoV, severe acute respiratory syndrome coronavirus. The alignment was generated using MultAlin multiple sequence alignment with hierarchical clustering (8).

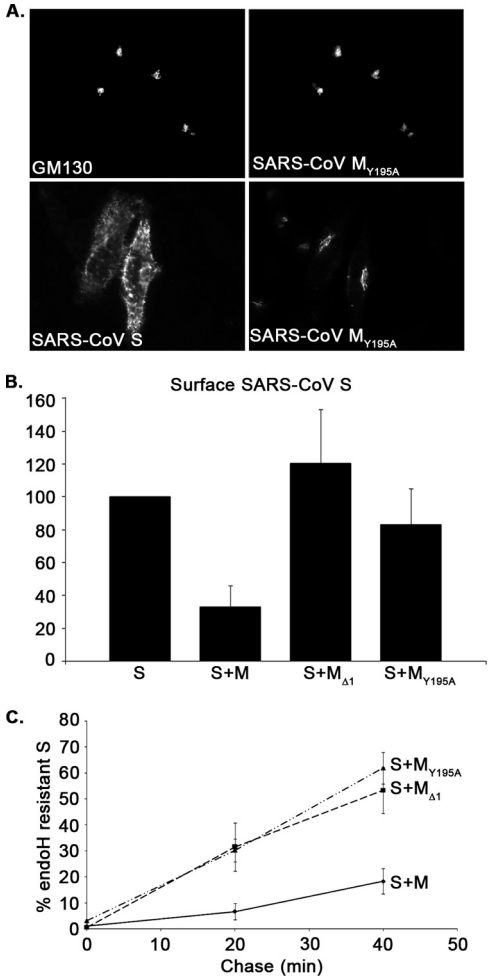

FIG. 8. Tyrosine 195 is important for efficient S and M interaction. (A) SARS-CoV M_{Y195A} localizes to the Golgi compartment but does not retain SARS-CoV S intracellularly. HeLa cells expressing SARS-CoV M_{Y195A} in the absence or presence of SARS-CoV S were stained as described for Fig. 3. The same field is shown for each horizontal set of panels. (B) SARS-CoV M_{Y195A} does not reduce the amount of SARS-CoV S at the plasma membrane. HEK293T cells exogenously coexpressing SARS-CoV S in the absence or presence of SARS-CoV M, $M_{\Delta 1}$, or M_{Y195A} were surface biotinylated as described for Fig. 3C. The averages of the results of three independent experiments ± standard errors of the means are shown. (C) SARS-CoV M_{Y195A} does not slow SARS-CoV S trafficking through the Golgi as well as wild-type SARS-CoV M does. HEK293T cells exogenously coexpressing SARS-CoV S and SARS-CoV M, $M_{\Delta 1}$, or M_{Y195A} were pulse-labeled and chased, and immunoprecipitated S protein was treated with endo H as described for Fig. 4. The averages of the results of three independent experiments ± standard errors of the means are shown.

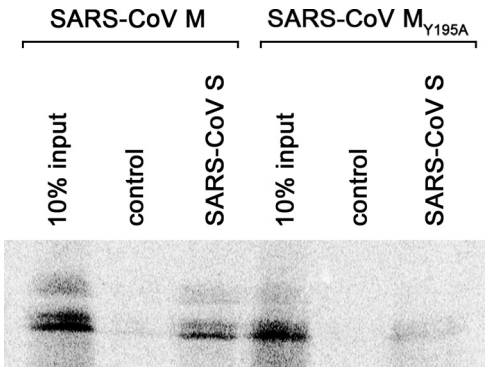

FIG. 9. Mutating Y_{195} disrupts the SARS-CoV S-M interaction *in vitro*. Equal amounts of solubilized *in vitro*-transcribed and -translated SARS-CoV M or M_{Y195A} were incubated with His-tagged SARS-CoV S prebound to nickel beads or with nickel beads alone. Samples were washed, subjected to SDS-PAGE, and visualized and quantified by phosphorimaging. Equal loading of recombinant S protein was ensured by staining with Coomassie blue (not shown).

phobic residue (5). This tyrosine-based motif is recognized by the clathrin adaptor proteins and mediates transmembrane protein endocytosis from the plasma membrane (5). The structure of the adaptor protein subunit responsible for binding the YXXΦ motif has been solved and highlights the importance of the tyrosine hydroxyl in hydrogen bonding, as well as its insertion in a hydrophobic binding pocket (46).

Although Y_{195} clearly plays a role in S-M interaction, it is unlikely to be the only region of SARS-CoV M that is important for interaction with S. When SARS-CoV S was expressed alone, 75% of S was resistant to endo H digestion after 40 min of chase. However, when M_{Y195A} was coexpressed with S, 60% of S was resistant to endo H digestion after 40 min (Fig. 4 and 8C). Although the ability of S and M_{Y195A} to interact was clearly and significantly reduced, S was not trafficked to the same extent as when it was expressed alone. Thus, it is likely that there is a region outside of the regions tested in this study that is also important for S-M interaction. Extra information could be either in the region of the tail not deleted in $M_{\Delta 2}$ or in the luminal or transmembrane domains. In support of this idea, Voss et al. recently implicated the N-terminal 134 amino acids of SARS-CoV M, which includes the transmembrane domains and a small portion of the cytoplasmic tail, in S-M interaction (60). The N-terminal 134 amino acids of M were able to retain S at the Golgi compartment by indirect immunofluorescence microscopy. The ability to interact with S was only measured by qualitative microscopy in that study. However, we did not observe Golgi retention of S with M containing residues M_1-R_{100} (M-G_{tail}, Fig. 1C). Since the SARS-CoV M cytoplasmic tail alone was able to retain S intracellularly (Fig. 1), the role of the transmembrane domains in S-M interaction remains unclear, and they may function primarily to present the cytoplasmic tail in the proper orientation.

The most extensive information on coronavirus S-M interaction comes from studies of MHV. The key regions for MHV S-M interaction have been mapped on both the S and M proteins (7, 11). Deletion of 70 amino acids in the amphipathic region of the MHV M cytoplasmic tail (residues 121 to 195) disrupts S-M interaction, as determined by indirect immunofluorescence microscopy and coimmunoprecipitation (11). Specific detergent combinations are needed to preserve MHV S-M interactions for coimmunoprecipitation (44). Here, we have used more sensitive assays to characterize the SARS-CoV S and M interaction. By using cell surface biotinylation and pulse-chase assays, we examined both steady-state localization and trafficking of SARS-CoV S to examine S-M interaction without the complication of maintaining S-M complexes in detergent lysates. Assays using virus-like particle (VLP) formation to assess contributions to virus assembly are often used to characterize coronavirus protein-protein interaction, although the exact requirements for VLP formation are controversial (3, 6, 10, 16, 26, 40, 44, 55, 59). However, in our hands, SARS-CoV S and M proteins were released in membrane vesicles from HEK293T and HeLa cells when expressed individually (data not shown), so we could not use this assay to study assembly.

We identified a different region of SARS-CoV M as involved in S interaction than was identified for MHV (11). Coronavirus M proteins are similar in size, ranging from approximately 220 to 260 amino acids. When the SARS-CoV M and MHV M protein sequences are aligned, Y_{195} is approximately 10 amino acids downstream in comparison to the 70 amino acids deleted in MHV studies. It is likely that the distance of the tyrosine from the membrane affects interaction with S. The coronavirus M protein cytoplasmic tail is considerably longer than that of the S cytoplasmic tail, but a large region of the M tail was shown to be tightly folded (2, 49, 50). Nevertheless, deletion of 70 amino acids from the MHV M tail could have altered the orientation and/or distance of a motif outside the 70-amino-acid stretch required for interaction with S. Importantly, the point mutations used here to dissect SARS-CoV S-M interaction are unlikely to disrupt overall features of the SARS-CoV M cytoplasmic tail.

Interestingly, in addition to the 70 amino acids deleted, a cytoplasmic tyrosine residue, Y_{211}, was shown to be important for MHV S and M interaction (11). Although S-M interaction was not fully abolished when Y_{211} was mutated to glycine in MHV M, MHV S-M interaction was severely reduced (11). MHV M Y_{211} is downstream in comparison to SARS-CoV M Y_{195}; however, when the analogous tyrosine in SARS-CoV M, Y_{205}, was mutated to alanine, it had no affect on S-M interaction as determined by the assays used here (data not shown). Although MHV M Y_{211} is outside of the 70 amino acids implicated in MHV S-M interaction, it clearly plays a role. This suggests that the spacing of the tail from the membrane may be important for S-M interaction and virus assembly.

Coronavirus S proteins form trimers prior to export from the ER, while M proteins form larger oligomers in the Golgi (13, 37). It is thought that coronavirus S-M interaction occurs in a pre-Golgi compartment, since endo H-sensitive proteins can be isolated by coimmunoprecipitation (42). It is possible that one S trimer could interact with multiple M oligomers, which could overcome a weak affinity through avidity. Indeed, if there are 16 to 25 M proteins for each S trimer, as estimated in recent cryoelectron microscopy (cryo-EM) studies of the SARS-CoV virion (41), only a fraction of M would be interacting with S. Although cryo-EM analyses of SARS-CoV and MHV virions did not detect a difference in the amounts of M proteins next to S spikes, it is not clear if a difference in packing

would be detectable at the resolution achieved in these studies. In addition, the C-terminal region of M interacts with the nucleocapsid protein N (14). Since the interaction site on M for S is also near the C terminus, it is possible that only M that is not associated with S is available for interaction with the viral nucleocapsid during assembly. Interestingly, the analogous region of the SARS-CoV M tail that was predicted to be tightly folded in MHV lacks the interaction sites for both S and N. This region may also be tightly folded in SARS-CoV M and could function to regulate the spacing of the C-terminal region from the membrane.

In conclusion, our results suggest that the SARS-CoV M cytoplasmic tail specifically retains the SARS-CoV S protein near the virus assembly site, and Y_{195} in the M cytoplasmic tail appears to be important for this interaction. Ongoing work is directed toward determining the region of SARS-CoV S that is recognized by this region of the M tail.

ACKNOWLEDGMENTS

This work was supported by National Institutes of Health grant R21 A1072312 and a Ford Foundation Predoctoral Diversity Fellowship.

The following reagents were obtained through the NIH Biodefense and Emerging Infections Research Resources Repository, NIAID, NIH: C-terminally histidine-tagged SARS-CoV spike (S) protein NR-686, a recombinant expressed from baculovirus, and monoclonal antibody anti-SARS-CoV S protein (similar to 341C) NR-617.

We thank Jie Li for constructing pCAGGS/VSV G and pCAGGS/SARS-CoV M-G_{tail}. We also thank members of the Machamer laboratory for helpful discussions and comments on the manuscript.

REFERENCES

1. **Armstrong, J., S. Patel, and P. Riddle.** 1990. Lysosomal sorting mutants of coronavirus E1 protein, a Golgi membrane protein. J. Cell Sci. **95**(Pt. 2)**:** 191–197.
2. **Barcena, M., G. T. Oostergetel, W. Bartelink, F. G. Faas, A. Verkleij, P. J. Rottier, A. J. Koster, and B. J. Bosch.** 2009. Cryo-electron tomography of mouse hepatitis virus: insights into the structure of the coronavirion. Proc. Natl. Acad. Sci. U. S. A. **106:**582–587.
3. **Baudoux, P., C. Carrat, L. Besnardeau, B. Charley, and H. Laude.** 1998. Coronavirus pseudoparticles formed with recombinant M and E proteins induce alpha interferon synthesis by leukocytes. J. Virol. **72:**8636–8643.
4. **Bisht, H., A. Roberts, L. Vogel, A. Bukreyev, P. L. Collins, B. R. Murphy, K. Subbarao, and B. Moss.** 2004. Severe acute respiratory syndrome coronavirus spike protein expressed by attenuated vaccinia virus protectively immunizes mice. Proc. Natl. Acad. Sci. U. S. A. **101:**6641–6646.
5. **Bonifacino, J. S., and L. M. Traub.** 2003. Signals for sorting of transmembrane proteins to endosomes and lysosomes. Annu. Rev. Biochem. **72:**395–447.
6. **Boscarino, J. A., H. L. Logan, J. J. Lacny, and T. M. Gallagher.** 2008. Envelope protein palmitoylations are crucial for murine coronavirus assembly. J. Virol. **82:**2989–2999.
7. **Bosch, B. J., C. A. de Haan, S. L. Smits, and P. J. Rottier.** 2005. Spike protein assembly into the coronavirion: exploring the limits of its sequence requirements. Virology **334:**306–318.
8. **Corpet, F.** 1988. Multiple sequence alignment with hierarchical clustering. Nucleic Acids Res. **16:**10881–10890.
9. **Corse, E., and C. E. Machamer.** 2002. The cytoplasmic tail of infectious bronchitis virus E protein directs Golgi targeting. J. Virol. **76:**1273–1284.
10. **Corse, E., and C. E. Machamer.** 2000. Infectious bronchitis virus E protein is targeted to the Golgi complex and directs release of virus-like particles. J. Virol. **74:**4319–4326.
11. **de Haan, C. A., M. Smeets, F. Vernooij, H. Vennema, and P. J. Rottier.** 1999. Mapping of the coronavirus membrane protein domains involved in interaction with the spike protein. J. Virol. **73:**7441–7452.
12. **de Haan, C. A., H. Vennema, and P. J. Rottier.** 2000. Assembly of the coronavirus envelope: homotypic interactions between the M proteins. J. Virol. **74:**4967–4978.
13. **Delmas, B., and H. Laude.** 1990. Assembly of coronavirus spike protein into trimers and its role in epitope expression. J. Virol. **64:**5367–5375.
14. **Fang, X., L. Ye, K. A. Timani, S. Li, Y. Zen, M. Zhao, H. Zheng, and Z. Wu.** 2005. Peptide domain involved in the interaction between membrane protein and nucleocapsid protein of SARS-associated coronavirus. J. Biochem. Mol. Biol. **38:**381–385.
15. **Gallagher, T. M., and M. J. Buchmeier.** 2001. Coronavirus spike proteins in viral entry and pathogenesis. Virology **279:**371–374.
16. **Godeke, G. J., C. A. de Haan, J. W. Rossen, H. Vennema, and P. J. Rottier.** 2000. Assembly of spikes into coronavirus particles is mediated by the carboxy-terminal domain of the spike protein. J. Virol. **74:**1566–1571.
17. **Gorbalenya, A. E., E. J. Snijder, and W. J. Spaan.** 2004. Severe acute respiratory syndrome coronavirus phylogeny: toward consensus. J. Virol. **78:**7863–7866.
18. **Herscovics, A.** 1999. Importance of glycosidases in mammalian glycoprotein biosynthesis. Biochim. Biophys. Acta **1473:**96–107.
19. **Hicks, S. W., and C. E. Machamer.** 2002. The NH2-terminal domain of Golgin-160 contains both Golgi and nuclear targeting information. J. Biol. Chem. **277:**35833–35839.
20. **Hofmann, H., K. Hattermann, A. Marzi, T. Gramberg, M. Geier, M. Krumbiegel, S. Kuate, K. Uberla, M. Niedrig, and S. Pohlmann.** 2004. S protein of severe acute respiratory syndrome-associated coronavirus mediates entry into hepatoma cell lines and is targeted by neutralizing antibodies in infected patients. J. Virol. **78:**6134–6142.
21. **Hogue, B., and C. Machamer.** 2008. Coronavirus structural proteins and virus assembly, p. 179–200. *In* S. Perlman, T. Gallagher, and E. Snijder (ed.), Nidoviruses. ASM Press, Washington, DC.
22. **Hsieh, Y. C., H. C. Li, S. C. Chen, and S. Y. Lo.** 2008. Interactions between M protein and other structural proteins of severe, acute respiratory syndrome-associated coronavirus. J. Biomed Sci. **15:**707–717.
23. **Huang, C., N. Ito, C. T. Tseng, and S. Makino.** 2006. Severe acute respiratory syndrome coronavirus 7a accessory protein is a viral structural protein. J. Virol. **80:**7287–7294.
24. **Huang, C., K. Narayanan, N. Ito, C. J. Peters, and S. Makino.** 2006. Severe acute respiratory syndrome coronavirus 3a protein is released in membranous structures from 3a protein-expressing cells and infected cells. J. Virol. **80:**210–217.
25. **Huang, C., C. J. Peters, and S. Makino.** 2007. Severe acute respiratory syndrome coronavirus accessory protein 6 is a virion-associated protein and is released from 6 protein-expressing cells. J. Virol. **81:**5423–5426.
26. **Huang, Y., Z. Y. Yang, W. P. Kong, and G. J. Nabel.** 2004. Generation of synthetic severe acute respiratory syndrome coronavirus pseudoparticles: implications for assembly and vaccine production. J. Virol. **78:**12557–12565.
27. **Ischiropoulos, H.** 2009. Protein tyrosine nitration—an update. Arch. Biochem. Biophys. **484:**117–121.
28. **Ito, N., E. C. Mossel, K. Narayanan, V. L. Popov, C. Huang, T. Inoue, C. J. Peters, and S. Makino.** 2005. Severe acute respiratory syndrome coronavirus 3a protein is a viral structural protein. J. Virol. **79:**3182–3186.
29. **Klumperman, J., J. K. Locker, A. Meijer, M. C. Horzinek, H. J. Geuze, and P. J. Rottier.** 1994. Coronavirus M proteins accumulate in the Golgi complex beyond the site of virion budding. J. Virol. **68:**6523–6534.
30. **Kuiken, T., R. A. Fouchier, M. Schutten, G. F. Rimmelzwaan, G. van Amerongen, D. van Riel, J. D. Laman, T. de Jong, G. van Doornum, W. Lim, A. E. Ling, P. K. Chan, J. S. Tam, M. C. Zambon, R. Gopal, C. Drosten, S. van der Werf, N. Escriou, J. C. Manuguerra, K. Stohr, J. S. Peiris, and A. D. Osterhaus.** 2003. Newly discovered coronavirus as the primary cause of severe acute respiratory syndrome. Lancet **362:**263–270.
31. **Kuo, L., K. R. Hurst, and P. S. Masters.** 2007. Exceptional flexibility in the sequence requirements for coronavirus small envelope protein function. J. Virol. **81:**2249–2262.
32. **Kuo, L., and P. S. Masters.** 2003. The small envelope protein E is not essential for murine coronavirus replication. J. Virol. **77:**4597–4608.
33. **Lamirande, E. W., M. L. DeDiego, A. Roberts, J. P. Jackson, E. Alvarez, T. Sheahan, W. J. Shieh, S. R. Zaki, R. Baric, L. Enjuanes, and K. Subbarao.** 2008. A live attenuated severe acute respiratory syndrome coronavirus is immunogenic and efficacious in golden Syrian hamsters. J. Virol. **82:**7721–7724.
34. **Larson, H. E., S. E. Reed, and D. A. Tyrrell.** 1980. Isolation of rhinoviruses and coronaviruses from 38 colds in adults. J. Med. Virol. **5:**221–229.
35. **Lefrancois, L., and D. S. Lyles.** 1982. The interaction of antibody with the major surface glycoprotein of vesicular stomatitis virus. II. Monoclonal antibodies of nonneutralizing and cross-reactive epitopes of Indiana and New Jersey serotypes. Virology **121:**168–174.
36. **Locker, J. K., J. Klumperman, V. Oorschot, M. C. Horzinek, H. J. Geuze, and P. J. Rottier.** 1994. The cytoplasmic tail of mouse hepatitis virus M protein is essential but not sufficient for its retention in the Golgi complex. J. Biol. Chem. **269:**28263–28269.
37. **Locker, J. K., D. J. Opstelten, M. Ericsson, M. C. Horzinek, and P. J. Rottier.** 1995. Oligomerization of a trans-Golgi/trans-Golgi network retained protein occurs in the Golgi complex and may be part of its retention. J. Biol. Chem. **270:**8815–8821.
38. **Lontok, E., E. Corse, and C. E. Machamer.** 2004. Intracellular targeting signals contribute to localization of coronavirus spike proteins near the virus assembly site. J. Virol. **78:**5913–5922.
39. **McBride, C. E., J. Li, and C. E. Machamer.** 2007. The cytoplasmic tail of the severe acute respiratory syndrome coronavirus spike protein contains a novel endoplasmic reticulum retrieval signal that binds COPI and promotes interaction with membrane protein. J. Virol. **81:**2418–2428.

40. **Mortola, E., and P. Roy.** 2004. Efficient assembly and release of SARS coronavirus-like particles by a heterologous expression system. FEBS Lett. **576:**174–178.
41. **Neuman, B. W., B. D. Adair, C. Yoshioka, J. D. Quispe, G. Orca, P. Kuhn, R. A. Milligan, M. Yeager, and M. J. Buchmeier.** 2006. Supramolecular architecture of severe acute respiratory syndrome coronavirus revealed by electron cryomicroscopy. J. Virol. **80:**7918–7928.
42. **Nguyen, V. P., and B. G. Hogue.** 1997. Protein interactions during coronavirus assembly. J. Virol. **71:**9278–9284.
43. **Niwa, H., K. Yamamura, and J. Miyazaki.** 1991. Efficient selection for high-expression transfectants with a novel eukaryotic vector. Gene **108:**193–199.
44. **Opstelten, D. J., M. J. Raamsman, K. Wolfs, M. C. Horzinek, and P. J. Rottier.** 1995. Envelope glycoprotein interactions in coronavirus assembly. J. Cell Biol. **131:**339–349.
45. **Ortego, J., J. E. Ceriani, C. Patino, J. Plana, and L. Enjuanes.** 2007. Absence of E protein arrests transmissible gastroenteritis coronavirus maturation in the secretory pathway. Virology **368:**296–308.
46. **Owen, D. J., and P. R. Evans.** 1998. A structural explanation for the recognition of tyrosine-based endocytotic signals. Science **282:**1327–1332.
47. **Petit, C. M., V. N. Chouljenko, A. Iyer, R. Colgrove, M. Farzan, D. M. Knipe, and K. G. Kousoulas.** 2007. Palmitoylation of the cysteine-rich endodomain of the SARS-coronavirus spike glycoprotein is important for spike-mediated cell fusion. Virology **360:**264–274.
48. **Rota, P. A., M. S. Oberste, S. S. Monroe, W. A. Nix, R. Campagnoli, J. P. Icenogle, S. Penaranda, B. Bankamp, K. Maher, M. H. Chen, S. Tong, A. Tamin, L. Lowe, M. Frace, J. L. DeRisi, Q. Chen, D. Wang, D. D. Erdman, T. C. Peret, C. Burns, T. G. Ksiazek, P. E. Rollin, A. Sanchez, S. Liffick, B. Holloway, J. Limor, K. McCaustland, M. Olsen-Rasmussen, R. Fouchier, S. Gunther, A. D. Osterhaus, C. Drosten, M. A. Pallansch, L. J. Anderson, and W. J. Bellini.** 2003. Characterization of a novel coronavirus associated with severe acute respiratory syndrome. Science **300:**1394–1399.
49. **Rottier, P., D. Brandenburg, J. Armstrong, B. van der Zeijst, and G. Warren.** 1984. Assembly in vitro of a spanning membrane protein of the endoplasmic reticulum: the E1 glycoprotein of coronavirus mouse hepatitis virus A59. Proc. Natl. Acad. Sci. U. S. A. **81:**1421–1425.
50. **Rottier, P. J., G. W. Welling, S. Welling-Wester, H. G. Niesters, J. A. Lenstra, and B. A. Van der Zeijst.** 1986. Predicted membrane topology of the coronavirus protein E1. Biochemistry **25:**1335–1339.
51. **Schaecher, S. R., J. M. Mackenzie, and A. Pekosz.** 2007. The ORF7b protein of severe acute respiratory syndrome coronavirus (SARS-CoV) is expressed in virus-infected cells and incorporated into SARS-CoV particles. J. Virol. **81:**718–731.
52. **Schwegmann-Wessels, C., M. Al-Falah, D. Escors, Z. Wang, G. Zimmer, H. Deng, L. Enjuanes, H. Y. Naim, and G. Herrler.** 2004. A novel sorting signal for intracellular localization is present in the S protein of a porcine coronavirus but absent from severe acute respiratory syndrome-associated coronavirus. J. Biol. Chem. **279:**43661–43666.
53. **Shen, S., P. S. Lin, Y. C. Chao, A. Zhang, X. Yang, S. G. Lim, W. Hong, and Y. J. Tan.** 2005. The severe acute respiratory syndrome coronavirus 3a is a novel structural protein. Biochem. Biophys. Res. Commun. **330:**286–292.
54. **Simmons, G., J. D. Reeves, A. J. Rennekamp, S. M. Amberg, A. J. Piefer, and P. Bates.** 2004. Characterization of severe acute respiratory syndrome-associated coronavirus (SARS-CoV) spike glycoprotein-mediated viral entry. Proc. Natl. Acad. Sci. U. S. A. **101:**4240–4245.
55. **Siu, Y. L., K. T. Teoh, J. Lo, C. M. Chan, F. Kien, N. Escriou, S. W. Tsao, J. M. Nicholls, R. Altmeyer, J. S. Peiris, R. Bruzzone, and B. Nal.** 2008. The M, E, and N structural proteins of the severe acute respiratory syndrome coronavirus are required for efficient assembly, trafficking, and release of virus-like particles. J. Virol. **82:**11318–11330.
56. **Song, H. C., M. Y. Seo, K. Stadler, B. J. Yoo, Q. L. Choo, S. R. Coates, Y. Uematsu, T. Harada, C. E. Greer, J. M. Polo, P. Pileri, M. Eickmann, R. Rappuoli, S. Abrignani, M. Houghton, and J. H. Han.** 2004. Synthesis and characterization of a native, oligomeric form of recombinant severe acute respiratory syndrome coronavirus spike glycoprotein. J. Virol. **78:**10328–10335.
57. **Swift, A. M., and C. E. Machamer.** 1991. A Golgi retention signal in a membrane-spanning domain of coronavirus E1 protein. J. Cell Biol. **115:**19–30.
58. **Thorp, E. B., J. A. Boscarino, H. L. Logan, J. T. Goletz, and T. M. Gallagher.** 2006. Palmitoylations on murine coronavirus spike proteins are essential for virion assembly and infectivity. J. Virol. **80:**1280–1289.
59. **Vennema, H., G. J. Godeke, J. W. Rossen, W. F. Voorhout, M. C. Horzinek, D. J. Opstelten, and P. J. Rottier.** 1996. Nucleocapsid-independent assembly of coronavirus-like particles by co-expression of viral envelope protein genes. EMBO J. **15:**2020–2028.
60. **Voss, D., S. Pfefferle, C. Drosten, L. Stevermann, E. Traggiai, A. Lanzavecchia, and S. Becker.** 2009. Studies on membrane topology, N-glycosylation and functionality of SARS-CoV membrane protein. Virol. J. **6:**79.
61. **Weisz, O. A., A. M. Swift, and C. E. Machamer.** 1993. Oligomerization of a membrane protein correlates with its retention in the Golgi complex. J. Cell Biol. **122:**1185–1196.
62. **WHO.** 2003. Summary of probable SARS cases with onset of illness from 1 November 2002 to 31 July 2003. Global Alert and Response (GAR), World Health Organization, Geneva, Switzerland. http://www.who.int/csr/sars/country/table2004_04_21/en/.
63. **Winter, C., C. Schwegmann-Wessels, U. Neumann, and G. Herrler.** 2008. The spike protein of infectious bronchitis virus is retained intracellularly by a tyrosine motif. J. Virol. **82:**2765–2771.
64. **Youn, S., E. W. Collisson, and C. E. Machamer.** 2005. Contribution of trafficking signals in the cytoplasmic tail of the infectious bronchitis virus spike protein to virus infection. J. Virol. **79:**13209–13217.